EFFICIENT USE OF NATURAL GAS IN STOVES – PAPER COB09-0553

Francisco Domingues Alves de Sousa, fdasousa@ipt.br
Ding Hua, ding@ipt.br
Instituto de Pesquisas Tecnológicas do Estado de São Paulo – IPT

EugenioPierrobon Neto, eneto@comgas.com.br
Companhia de Gás de São Paulo – Comgas

Abstract. *This paper presents the results of a work concerning energy optimization in cooking processes accomplished in industrial stoves, comprising two steps: mathematical modeling of the radial jet which originates the flame and experimental work, in which the effects on thermal efficiency of several devices (thermal radiation shields) and surface treatment were tested showing that the efficiency achieved for large kettles (height/diameter = 1,0) involved by aluminum shields, both of them blackened by soot deposition, was nearly 20% higher than that measured for the same recipient without any surface treatment and not shielded. For a shielded saucepan or casserole, with the same diameter, the same surface treatment but having the ratio (height/diameter = 0,5), the efficiency improvement compared to the reference configuration was a little bit lower: 17%. Kettle and saucepan bottom blackening solely resulted efficiency improvements around 9,0%. The mathematical model showed itself quite good in predicting the experimental results at least in a qualitatively fashion.*

Keywords*: energy saving, stoves, small natural gas burners*

1. INTRODUCTION

Large industrial equipment, like boilers, still furnaces for petrochemical operations, reheating furnaces for steel slabs, etc. have efficiencies in the range 75 to 90% and despite the small potential for efficiency improvements, a lot of research work has been done in the last 25 years addressed to this subject. On the other hand, domestic and industrial stoves have typical efficiencies in the range 50 to 60% and despite the large potential for efficiency improvements, very little research work has been done in the same period. This evidence was the motivation for the present work. A look over the cooking operation reveals the main causes of its inefficiency as shown in Fig. 1.

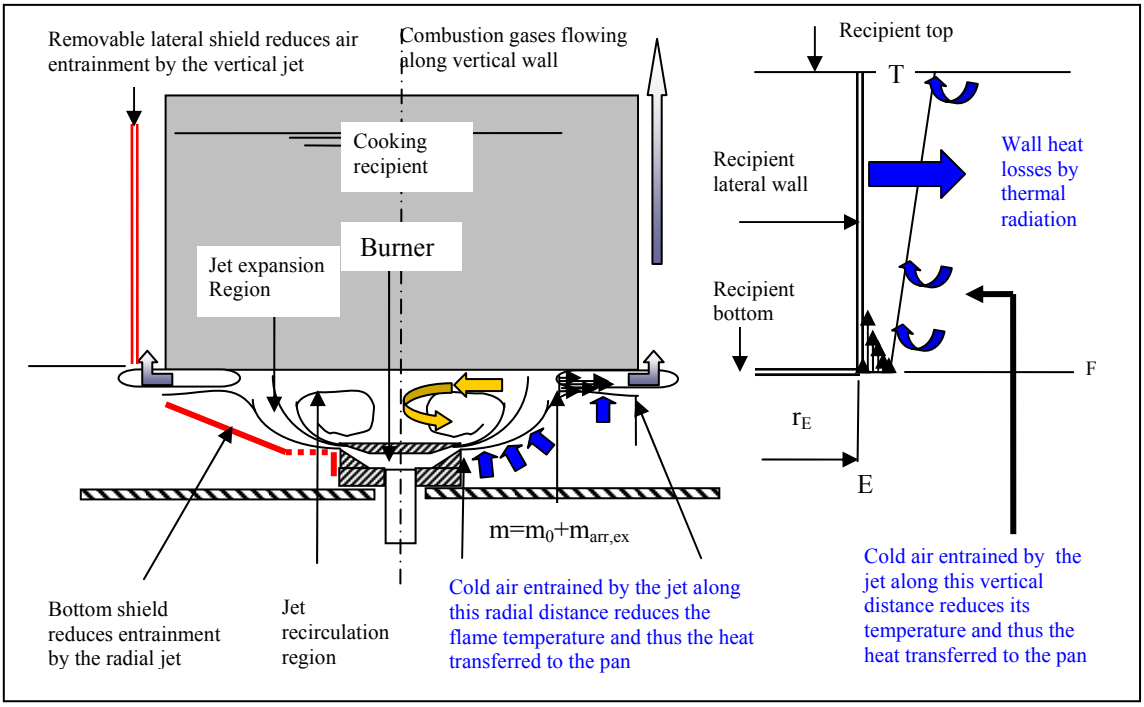

Figure 1. Main causes of inefficiency in cooking operations in stoves

Once the main inefficiencies have been identified, a natural solution seems to be the adoption of shields bellow the radial jet expansion region and along the lateral kettle wall, as shown in the same figure. These shields accomplish two functions: reduce the radiation losses and the flow rate of cold air drawn into the hot gas jets either in the radial or in the

vertical sections. The theoretical and experimental study of the effect of these solutions jointly with surface treatments was the subject of the present work.

2. MATHEMATICAL MODELING

The mathematical model equates the three regions of the jet expansion shown in Fig. 1: i) region of the radial jet (flame), from r_0 to r_R (radius of adherence circle), ii) expansion of the adhered radial jet from r_R to r_E (radius of the recipient bottom) and iii) expansion of the axial jet adhered to the recipient lateral wall, from F to T.

2.1. Jet expansion region i

Briefly, the model allows the determination of the following parameters in region i: adherence circle radius (r_R), total jet flow rate at the adherence circle (Q_t), entrained cold air flow rate by the lower part of the jet ($Q_{arr,ex}$ and $m_{arr,ex}$), flow rate of hot recycled gases entrained by the jet upper part ($Q_{arr,in}$ and $m_{arr,in}$), heat exchanged among the recycled gases and the recipient bottom ($W_{0\text{-}R}$), recycled gases temperature as entrained by the jet (T_b) and jet mean temperature at the adherence circle (T_R). This former part of the jet was modeled using the same approach and nomenclature used in the paper of Page et al.(1988), as shown in Fig. 2. The most important equations in this part are:

$$C_p = (P_b - P_\infty)/(0{,}5 * \rho_0 * u_0^2) \tag{1}$$

$$\Delta = -2/(C_P * R_0) * (\cos\theta_0 - \cos\theta_R) * [1 - 4 * (sen\theta_R - sen\theta_0)/(R_0 * C_P)]^{-0{,}5} \tag{2}$$

$$R_R^2 = 1 - 4 * (sen\theta_R - sen\theta_0)/(R_0 * C_P) \tag{3}$$

$$\left(Q_t(r_R)/Q_{0t}\right)^3 = 1 - 71{,}9764 * (\theta_R - \theta_0) * \left(2 * \pi * r_R * \upsilon/(C_P * Q_{0t})\right) \tag{4}$$

In Eq. (1), the parameter C_p, is called "pressure coefficient". Once P_b and P_∞ are considered uniform and the values ρ_0, u_0 and P_∞ are given, if it is possible to measure P_b, it will be possible to calculate C_p. Eq. (2) allows the calculation of θ_R (the angle formed by the jet bend axis and the recipient bottom - Fig.3), in this equation: $\Delta = x_p/r_0$ (dependent only on geometry) and $R_0 = r_0/b$. Once θ_R is calculated it can be introduced into Eq. (3), allowing the calculation of R_R ($R_R = r_R/r0$) and, therefore, r_R (radius of the adherence circle).

Equation (4), derived from the momentum conservation, when applied to the adherence circle ($\theta = \theta_R$ and $r = r_R$), allows the calculation of the total jet flow rate, Q_t, over that circle and, therefore, the flow rate of external air plus that of recycled gases entrained by the jet ($Q_t - Q_{0t}$), where Q_{0t} is the volumetric flow rate of the mixture (primary air + NG) issuing from the burner slit. The total flow rate entrained by the jet ($Q_{arr} = Q_t(r_R) - Q_{0t}$) is composed by two terms: that one entrained by its internal side, $Q_{arr,in}$ and the other entrained by its external side, $Q_{arr,ex}$, their values being related by Eq. (5), which was proposed in an earlier paper given by Sawyer (1963).

$$Q_{arr,in} = 0{,}71 * Q_{arr,ex} \tag{5}$$

From this equation it is possible to calculate the flow rates entrained by both sides of the jet, using the two expressions of Eq. (6), where ρ_b and ρ_∞ are the densities of the recycled gases and the air respectively

$$m_{arr,in} = \frac{0{,}71 * \rho_\infty * \rho_b}{0{,}71 * \rho_b + \rho_\infty} * Q_{arr}\,; m_{arr,ex} = \frac{\rho_\infty^2}{0{,}71 * \rho_b + \rho_\infty} * Q_{arr} \tag{6}$$

As the jet strikes the adherence circle it is split in two plane radial jets, the former flowing to center direction ($m_{arr,in}$) and the second flowing to the recipient bottom rim, which flow rate is $m_0 + m_{arr,ex}$, (Fig. 1). The above description is enough to establish mass and energy balances along the first region of the jet: Eq. (7), (8) and (9). In Eq.(7), PCS_{GN} is the higher calorific value for natural gas (52040 kJ/kg) and in Eq. (9), $W_{0\text{-}R}$ is the heat exchanged among the recycled gases and the recipient bottom, inside the circle having radius r_R.

$$m_{arr,in} * C_{p,b} * (T_b - T_{ref}) + m_{GN} * PCS_{GN} = m_R * C_{p,R} * (T_R - T_{ref}) \tag{7}$$

$$m_R = m_0 + m_{arr,in} + m_{arr,ex} \tag{8}$$

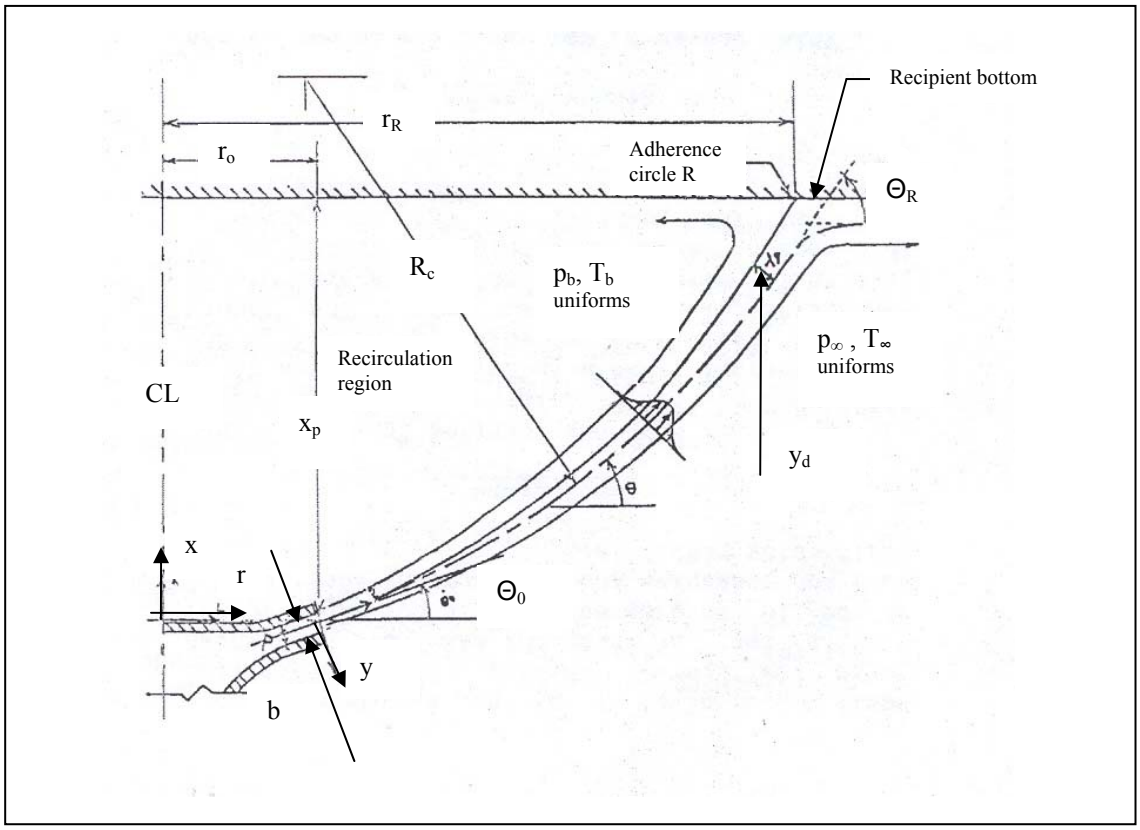

Figure 2. Nomenclature for the jet expansion region r_0 - r_R

$$m_{arr,in} * C_{p,b} * (T_R - T_b) = W_{0-R} \tag{9}$$

2.2. Heat exchanged among the jet and the recipient bottom (circle radius r_R)

Ostowari et al (1988) have established relations between the Stanton number and the non-dimensional parameter *(r/r0)*, called r_b in that work, for values of the last one lying between 0 and 4,0, the jet discharging angle θ_0 = -10, 0, +10 e +45º, the non-dimensional parameter x_p/b (3, 4, 6 e 8) and four Reynolds number at the slit jet (1760, 3530, 5290, 7060). Fig. 3 shows one such a graphic from the set presented in that paper, referred to θ_0=0º and x_p/b=3. The Stanton number is defined by Eq. (10), in which *St* and *h* are local values (for a definite value r/r_0); however the values of density, specific heat and velocity are referred to the nozzle discharge condition.

$$St = h/(\rho_0 * C_{p,0} * u_0) \tag{10}$$

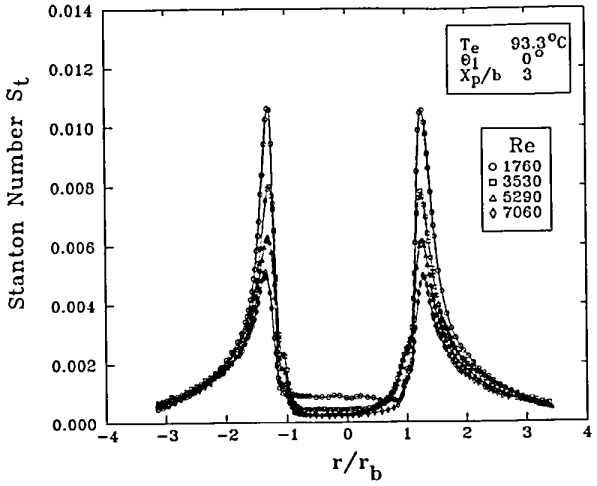

Figure 3. Stanton number X *(r/r0)* for *(xp/b)* = 3 [Ostowari et al (1988)]

From these data, the easier way to obtain h from Eq. (10) is to fit functions $St = St\ (r/r_0)$ to them. Finally, it is possible to calculate $W_{0\text{-}R}$, from Eq. (9), using finite-differences Δr in the r range (0 - r_R) and using Eq. (11) and (12). In Eq. (11), T_p represents the recipient bottom temperature.

$$dW_r = 2 * \pi * r * \Delta r * h(r / r_0) * [T(r) - T_P] \tag{11}$$

$$dW_r = m_{arr,in} * C_{p,b} * \Delta T_r \tag{12}$$

2.3. Jet expansion region ii - along r_R - r_E

The important equations in this part are:

$$Q_{rR,R\to E} = Q_{0t} + Q_{arr,ex} = Q_{0t} + 0{,}585 * (Q_t - Q_{0t}) = 0{,}585 * Q_t + 0{,}415 * Q_{0t} \tag{13}$$

$$\left(s / r_0\right)^{2/3} = 0{,}0917 * \left(Q_t / Q_{0t}\right)^2 * \left(Q_{0t} * b / (2 * \pi * r_R^3 * \upsilon)\right)^{2/3} \tag{14}$$

$$U(s) = 0{,}4543 * \left(J^2 / (\rho^2 * \upsilon * s)\right)^{1/3} \tag{15}$$

$$J = J_0 * \left(r_0 / r_R\right) \tag{16}$$

$$U(s) = K / \sqrt{s} \Rightarrow K = U(s) * \sqrt{s} \Rightarrow\ U(E) = K / \sqrt{s + (r_E - r_R)} \tag{17}$$

$$q(E) = q(R) + (K / \Omega) * (\sqrt{s + r_E - r_R} - \sqrt{s}) \Rightarrow Q(E) = q(E) * 2 * \pi * r_E \tag{18}$$

$$Q_{arr,R\to E} = Q(E) - Q_{rR,R\to E} \tag{19}$$

Eq. (13) is obtained from Eq. (5). Eq. (14) comes, from the paper of Page et al (1988) and allows the calculation of s value (distance from the adherence circle to the r_0 radius circle, measured along the bend jet axis – see Fig. 3). With this value it is possible to calculate the maximum velocity of the half-jet ($R \rightarrow E$), at the point R, $U(s)$ using Eq. (15), in which J is the momentum, by unity of jet perimeter (round), at abcissa s, calculated by Eq. (16), in which J_0 is the jet momentum, by unity of slit perimeter (radius r_0). Eq. (17) proposed by Abramovich (1963), allows the calculation of the constant for the jet center-line velocity decaying, K (left side), and with its right side one can calculate the velocity at the circle r_E, $U(E)$, for the half-jet ($R \rightarrow E$):

In the same abcissa (rim of recipient bottom) the volumetric flow rate by perimeter unity, disregarding the difference among the inner and outer perimeters, can be calculated using the left side of Eq. (18), proposed by Sawyer (1963), in which Ω is the parameter of the jet expansion (non-dimensional); its experimental value is 7,67. The total volumetric flow rate, $Q(E)$, at the bottom rim can be calculated by the right side of the same equation.

Finally the air flow rate entrained by the under side of the jet is calculated by Eq. (19), in which $Q_{rR,R\to E}$ is obtained from Eq. (13).

2.3.1. Energy balance in the jet region ii

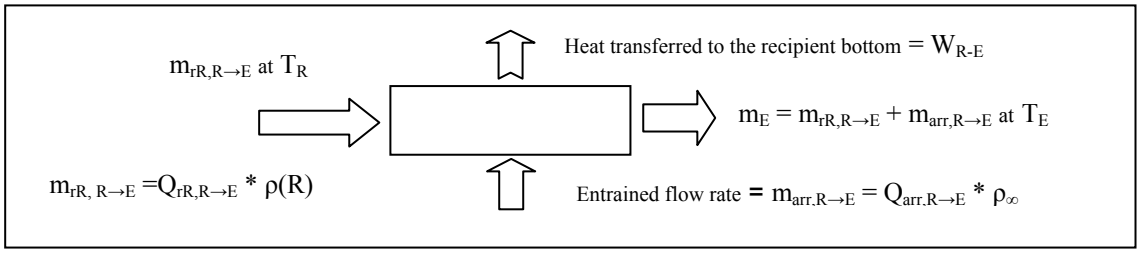

Figure 4 – Block diagram - energy balance in the region R-E

Important relations in this region are Eq. (20) to (23).

$$m_{rR,R\to E} * C_{p,R} * \left(T_R - T_\infty\right) - W_{R-E} = \left(m_{rR,R\to E} + m_{arr,R\to E}\right) * C_{p,E} * \left(T_E - T_\infty\right) \tag{20}$$

$$\Delta W_r = 2 * \pi * r * \Delta r * h(r / r_0) * [T(r) - T_P] \tag{21}$$

$$T_{r+\Delta r} = [m_{rR,R\to E} * C_{p,R} * (T_R - T_\infty)] / [(m_{rR,R\to E} + \Delta m_r) * C_{p,R}] + T_\infty \tag{22}$$

$$\Delta m_r = [2 * \pi * r_R * \rho_\infty * K / (2 * \Omega * \sqrt{s + n * \Delta r})] * \Delta r \tag{23}$$

The former is the energy balance equation that allows the determination of T_E, once W_{R-E} has been determined. This value will be determined dividing the r interval, $r_R - r_E$, in finite differences, Δr, and calculating, in each one, the heat exchanged by Eq.21, using $h(r/r_0)$ values obtained from equations adjusted to curves like that of Fig. 4. Equation (22) is used to calculate the temperature of the next volume element, once the later one is known; it needs the flow rate of cold air entrained into this jet element which is calculated by Eq. (23).

2.4. Jet expansion region iii

Without lateral shield the half-jet expands entraining cold air as the same time it exchanges heat with the lateral recipient wall. This expansion will be treated identically to the region ii, using proper equations for this region.

$$T_n = [m_{n-1} * C_{p,n} * (T_{n-1} - T_\infty) - \Delta W_n] / [(m_{n-1} + \Delta m_n) * C_{p,n}] + T_\infty \tag{24}$$

$$\Delta m_n = 2 * \pi * r_E * \rho_\infty * K / [2 * \Omega * \sqrt{s + (r_E - r_R) + (n-1) * \Delta x}] * \Delta x \tag{25}$$

$$\Delta W_n = 2 * \pi * r_E * \Delta x * h_n * [T_{n-1} - T_P] \tag{26}$$

$$W_{F-T} = \sum_1^N \Delta W_n \tag{27}$$

$$m_{F-T} = 2 * \pi * r_E * \rho_\infty * (K / \Omega) * (\sqrt{s + (r_E - r_R) + x_T} - \sqrt{s + (r_E - r_R)}) \tag{28}$$

$$U(x) = U(E) * \sqrt{[s + (r_E - r_R)] / [s + (r_E - r_R) + x]} \tag{29}$$

$$W_{perdas} = (2 * \pi * r_E * x_P) * \varepsilon_P * \sigma * (T_P^4 - T_\infty^4) \tag{30}$$

Equation (24) is the energy balance for the nth jet volume element, allowing the calculation of the gas exit temperature, once the temperature of the previous one is known, as well as its air entrained flow rate, Δm_n, which is calculated by Eq. (25) and the heat exchanged between this gas element and the corresponding element of the wall, which is calculated by Eq. (26). Equations (27) and (28) allow the calculation of the total heat exchanged and the total air flow rate entrained by the vertical jet. In Eq. (26), h_n is calculated by classical expressions for heat transfer by convection, using the maximum jet velocity in each section, $U(x)$ given by Eq. (29) as being the far away velocity (u_∞).

At the same time the vertical wall receives heat from the gaseous jet, it losses heat to the environment by radiation, which is calculated by Eq. (30), where σ is the Stefan-Boltzman constant = 5,767*10^{-11} [kW/(m^2.K^4)] and ε_P is the wall emissivity. Then the total net heat received by the wall is the difference ($W_{F-T} - W_{perdas}$).

2.5. Shield efects

Mounting a shield around a recipient, as shown in Fig. 1, has the effects shown in Fig. 5, in which an element resulting from division of the total height x_T into N parts is represented. The set of equations to represent the interactions among recipient, gases, shield and environment is shown in sequence.

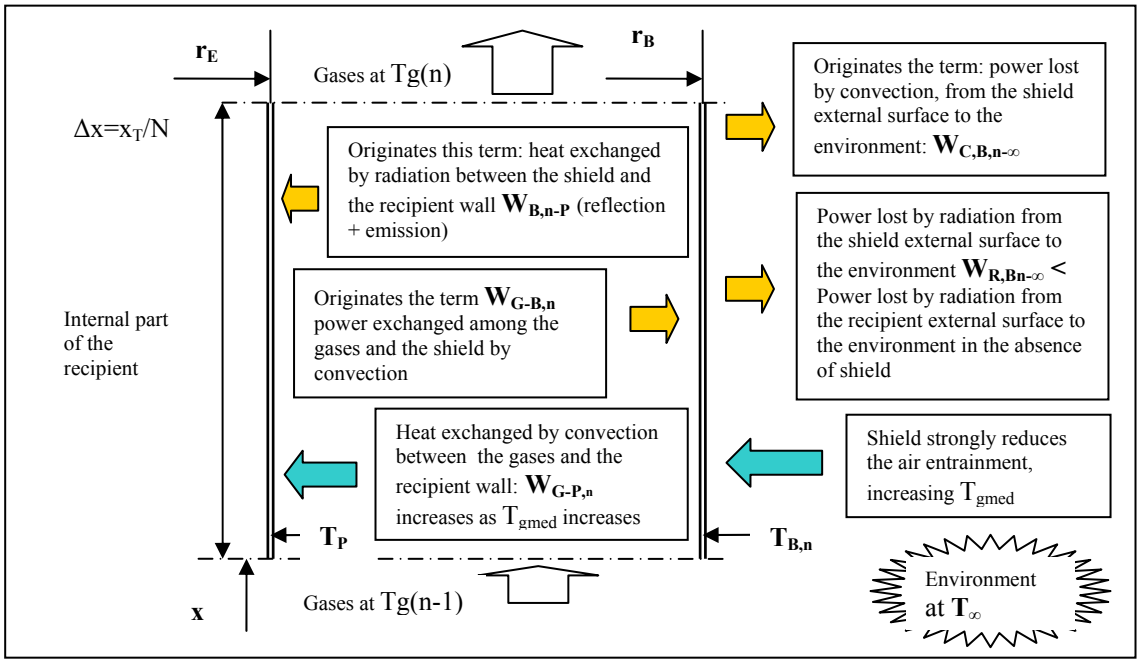

Figure 5 – Schematic representation of the interactions among gases, recipient, shield and environment

$$W_{G-P,n} = (2*\pi*r_E*\Delta x)*h_n*(T_{G,n-1}-T_P) \Rightarrow W_{G-B,n} = (2*\pi*r_B*\Delta x)*h_n*(T_{G,n-1}-T_{B,n}) \quad (31)$$

$$m_G*c_{pG,n-1}*(T_{G,n}-T_{G,n-1}) = -(W_{G-P,n}+W_{G-B,n}) \quad (32)$$

$$W_{G-B,n} = W_{B,n-P}+W_{C,B,n-\infty}+W_{R,B,n-\infty} \quad (33)$$

$$W_{C,B,n-\infty} = (2*\pi*r_B*\Delta x)*h_{e,n}*(T_{B,n}-T_\infty) \quad (34)$$

$$W_{R,B,n-\infty} = (2*\pi*r_B*\Delta x)*\varepsilon_B*\sigma*(T_{B,n}^4-T_\infty^4) \quad (35)$$

$$W_{B,n-P} = (S_B S_P)*\sigma*(T_{B,n}^4-T_P^4) \quad (36)$$

$$S_B S_P = \frac{A_P*\varepsilon_P}{1-\varepsilon_P}*\frac{A_B*\varepsilon_B}{1-\varepsilon_B}*\frac{s_P s_B}{\frac{A_P}{1-\varepsilon_P}*\left(A_B*\frac{\varepsilon_B}{1-\varepsilon_B}+\frac{A_P}{A_B}*s_P s_B\right)-{s_P s_B}^2} \quad (37)$$

Both sides of Eq. (31) represent the heat transferred from the gas flow to the lateral recipient wall and to the shield internal surface, by convection. Equation (32) represents the energy balance on the nth gas element. Equation (33) represents the energy balance on the nth shield element where the first term of the left side represents the heat exchanged between the nth elements of the shield and the recipient wall, calculated by Eq. (36). The last two terms of the left side of Eq. (33) are calculated by Eq. (34) and (35) which represent heat losses by the shield external surface to the environment, by convection and by radiation respectively. To solve this set of equations for each of the *N* elements, an iterative procedure was adopted.

Equation (37) represents the so-called global (or total) area for radiation heat transfer between two rings, according to Hottel (1967). This expression does not enter the reiterative procedure mentioned above, as it involves only geometry and radiative properties of the surfaces that were supposed not to vary in the temperature range considered. In this equation, $A_P = 2*\pi*r_E*\Delta x$, $A_B = 2*\pi*r_B*\Delta x$ and $s_P s_B$ is the so-called direct area for radiation heat

transfer between two rings, calculated as $s_P s_B = A_P * F_{P\text{-}B}$, where $F_{P\text{-}B}$ is the radiation factor between these surfaces, calculated from Howell (1997).

3. EXPERIMENTAL WORK

Several shields differing in conception (single or double wall), materials (stainless steel and aluminum), with external thermal insulation or not and the deposition of a tin soot layer over the external surface of the recipients or over the internal surface of the shields were tested against the reference configuration. Reference configuration means the recipient alone, without any surface treatment, heated by the gas flame according to the conventional practice. The main shield geometries which were tested are represented in Fig. 6 and Tab. 1.

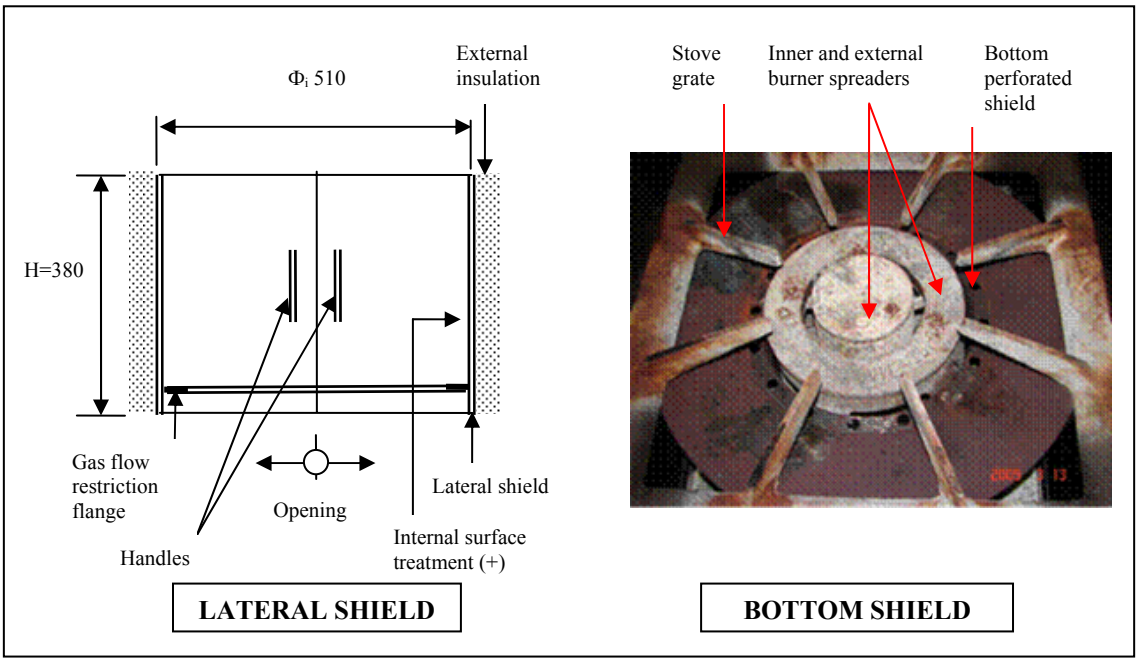

Figure 6 – Shields tested during experimental work

Table 1. Summary of the trials accomplished

Configuration nº	Shell	Internal shield surface treatment (+)	External shield insulation	Flange (*)	Recipient external surface treatment
1 (lateral) (#)	Double - stainless	Polished	no	no	none
2 (lateral) (#)	Single - stainless	Polished	Yes (**)	no	none
3 (lateral) (#)	Double – stainless	Blackened by soot	no	no	none
4 (lateral) (#)	Single - aluminum	polished	Yes (**)	no	none
5	This shield has not been built				
6 (bottom)	Single – low C steel	As rolled	no	-	none
7 (lateral) (#)	Double - aluminum	Polished	no	no	none
8 (lateral) (#)	Double - aluminum	Polished	no	yes	none
9 (lateral) (#)	Single - aluminum	Polished	Yes (**)	yes	none
10 (lateral) (#)	Single - aluminum	Blackened by soot	Yes (**)	yes	none
10a (lateral) (#)	Single - aluminum	Blackened by soot	Yes (**)	yes	Blackened by soot (lateral surface only)
10b (lateral) (#)	Single - aluminum	Blackened by soot	Yes (**)	yes	Blackened by soot (total external surface)
11 (lateral) @	Single - aluminum	Polished	Yes (**)	yes	none
12 (lateral) @	Single - aluminum	Blackened by soot	Yes (**)	yes	Blackened by soot (total external surface)
13 @	none	-	-	-	Blackened by soot (only the bottom)

(*) Gas flow restriction flange (see Fig. 6) (#) Large kettle (see Fig.7) @ sauce pan (see Fig.7)
(**) ½" thick ceramic fiber blanket (+) see Fig. 6

3.1. Stove burner throughput and recipients dimensions

The burners that equipped the stoves used for the trials were built with two gas-air mixtures spreaders, inner and peripheral, as shown in Fig. 6 (right side), both of them with 8,1 kW throughput. In all trials described in Tab. 1, only the external burner spreader was lighted.

As recommended by the standards for measurement of stove burner efficiency later described, the dimensions of the recipients were chosen according to the burner throughput, leading to the dimensions shown in Fig. 7.

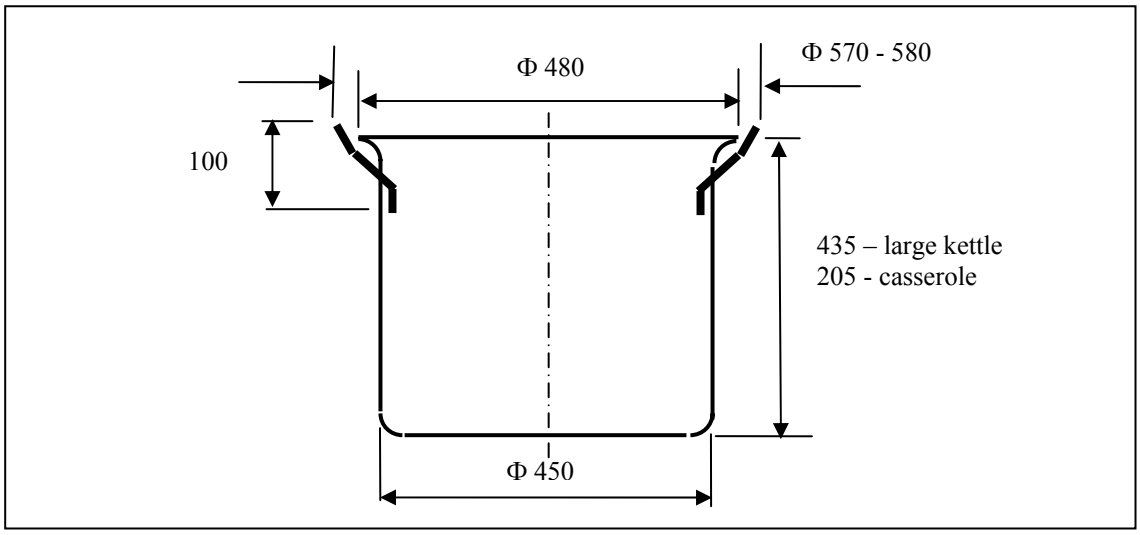

Figure 7. Dimensions of the recipients used in the efficiency tests

3.2. Proceedings and standards adopted for the tests

Two standards were used: the Brazilian NBR 13.723-2 "Aparelho doméstico de cocção a gás – Parte 2: Uso Racional de Energia" and the European EN 203-2-1:2006 "Gas heated catering equipment - Part 2-1: Specific requirements – open burners and wok burners". The last one was used because the former does not cover the power range of industrial catering equipment. All the requirements prescribed by those standards were satisfied except the room temperature (inside which the stoves were installed) because it was not equipped with conditioned air, so the environment temperature was allowed to vary along the successive trials. In order to compensate for these variations which affect the efficiency, the reference trials and those corresponding to the configuration to be tested (6 to 12 trials each) were interpolated. With this procedure the environment changes affected almost in the same way both sets of trials. For each new shield configuration, a new set of reference trials were accomplished and its mean efficiency value was than compared with the mean value of the trials corresponding to that configuration. Obviously the mean efficiency value for each reference set of trials resulted different. The number of trials in each set was determined from an early pilot set for which the minimum number was calculated to assure that the mean value was in a range smaller than 2% of this mean with 95% of confidence.

Roughly the test consists in heating a definite amount of water (defined for each recipient size) from an initial temperature of 20ºC (± 1ºC) until 90ºC (± 1ºC), the efficiency being calculated as the ratio of the heat supplied to the recipient (equivalent mass x specific heat) and the heat released by the fuel combustion (gas mass consumed x high calorific value).

3.3. Experimental results

For the early configurations 1 to 4 and 7 (see Tab.1), which were not provided by the gas flow restriction flange, the mean efficiencies obtained for each reference set of trials and those corresponding to the configuration being tested were statistically equal. In other words these configurations had not shown efficacy in increasing the efficiency counteracting the predictions made by the mathematical model.

After an extensive and troublesome investigation it was concluded that this contradiction was due to the disregard, in the mathematical model, of the buoyant forces along the two developing regions of the jet, namely the flame region and the flat radial jet adherent to the recipient bottom, which cause considerable increasing into the cold air flow rate entrained by the jet, thus cooling these parts that are just the hotter ones along the total jet path, when a shield is mounted around the recipient. It is important to keep in mind that this increasing into the cold air entrained by the jet along its path under the recipient bottom occurred simultaneously to a stronger decreasing into the cold air flow rate entrained along the vertical part of the jet developing adhered to the lateral recipient wall just due to the shield mounting.

As long as this problem was recognized and lately proven by experiment it was decided to adopt the gas flow restriction flange (see Fig. 6, left side) which partially solved it. In benefit of concision the steps of this investigation work are omitted in this paper. The results obtained for kettles and saucepans, for those configuration shields and surface treatments considered more promising, are shown in Tab. 2 below. As this table is quite resumed and for the sake of clarity, Tab. 3, presented later, shows details of the trials corresponding to the configuration nº 8, as an example.

Table 2. Efficiency improvements due to different shield configurations

Configuration nº	Mean efficiency value for reference trials set (a)	Mean efficiency value for the configuration trials set	Efficiency increasing [%]
8 (kettle)	0,530	0,583	10,0
9 (kettle)	0,527	0,589	11,7
10 (kettle)	0,520	0,584	12,3
10a (kettle)	0,528	0,604	14,4
10b (kettle)	0,538	0,641	19,1
11 (sauce pan)	0,471	0,494	4,9
12 (sauce pan)	0,489	0,572	17,0
13 (sauce pan)	0,486	0,531 (b)	9,3

(a) For each configuration a new set of reference trials was accomplished, resulting different mean efficiency values, due to changes in environment conditions (in all reference trials no shield was used nor surface treatments were applied).
(b) This configuration consists solely into the sauce pan bottom blackening by soot deposition (without lateral shield). This shows the important effect of surface emissivity.

Table 3. Description of the efficiency results for shield nº 8

Shield nº 8 - reference trials set					Shield nº 8 - configuration tials set				
Trial nº	date	start time	final time	Efficiency	Trial nº	date	start time	final time	Efficiency
1	02/12/08	8:51	9:32	0,535	1	02/12/08	9:46	10:24	0,577
2	02/12/08	10:40	11:21	0,537	2	02/12/08	11:36	12:14	0,591
3	02/12/08	14:37	15:17	0,540	3	02/12/08	15:35	16:13	0,570
4	03/12/08	8:49	9:34	0,513	4	03/12/08	9:51	10:29	0,582
5	03/12/08	10:48	11:29	0,527	5	03/12/08	11:42	12:20	0,579
6	03/12/08	13:50	14:32	0,528	6	03/12/08	14:45	15:22	0,584
7	03/12/08	15:41	16:22	0,524	7	04/12/08	10:16	10:56	0,573
8	04/12/08	9:19	10:02	0,497	8	04/12/08	12:07	12:45	0,586
9	04/12/08	11:12	11:53	0,528	9	04/12/08	14:15	14:52	0,593
10	04/12/08	15:13	15:53	0,540	10	04/12/08	16:14	16:51	0,591
11	05/12/08	9:15	9:56	0,536	11	05/12/08	10:10	10:48	0,587
12	05/12/08	11:05	11:45	0,545	12	05/12/08	11:56	12:33	0,591
13	05/12/08	14:18	14:58	0,541	13	05/12/08	15:13	15:51	0,570
Efficiency mean value				0,530	Efficiency mean value				0,583
Standard mean deviation				0,013	Standard mean deviation				0,008

It is important to notice the interpolation in the starting times for the trials of both sets, as to minimize environment conditions effects.

4. COMPARISON OF EXPERIMENTAL VALUES AND THOSE PREDICTED BY THE MODEL

The burners that equipped the stoves used for the experimental work have the following dimensions and correlated parameters used in the model: external radius of the gas-air mixture spreader, r_0 = 0,088 m; equivalent slit width, b = 0,001 m; angle between the jet exit and the recipient bottom plane, θ_0 = 0º; distance from the slit plane to the recipient bottom, x_p = 0,050 m; $\Delta = x_p/r_0$ = 0,571; $R_0 = r_0/b$ = 82,869 and the recipients (kettles and sauce pans) have radius, r_E = 0,225 m.

On a previous set of trials, operating the burner without flame, the following values, needed for the mathematical model were measured and calculated: gas-air mixture flow rate at atmospheric conditions, Q_{0t} = 0,002 m^3/s (5,457 m^3/h); gas-air mixture density, ρ_0 = 1,037 kg/m^3 and gas-air mixture velocity at the slit, u_0 = 2,611 m/s.

Introducing these values into the mathematical model it was possible to obtain, among other results, those listed in Tab. 4, with which its is possible to draw some few comparisons: For instance, the model predicts that the total net power received by the recipient (at the water boiling point) is improved from 2,460 kW to 2,641 kW due to the shielding with a single polished plate, which means an improvement of 7,4%. At the experimental work, the efficiency

increasing obtained with configuration Nº8 (shield consisting of two parallel plates, as shown in Tab. 1) was 10,0 % (see Tab. 2); so the agreement between the results is quite good.

Table 4. Values predicted by the mathematical model and measured in the trials

Parameter	predicted by the model		measured values (#)	
	no shield	with shield	no shield	with shield
Power exchanged between the recycled gases and the recipient bottom (W0-R) [kW]	1,207			
Power exchanged between the jet and the recipient bottom, region R-E, WR-E [kW]	0,811			
Total power supplied to the recipient bottom (W0-R + WR-E) [kW]	2,018			
Combustion gases temperature at recipient bottom rim, TE [ºC]	488		510 (*)	520 (*)
Power lost by the recipient lateral wall, without shield, Wperdas [kW]	0,013			
Net power received by the recipient lateral wall [kW]	0,442	0,623		
Total net power received by the recipient at the water boiling point [kW]	2,460	2,641		
Fraction of the total power thet is received by the lateral wall [%]	17,968	23,585		
Gases temperatura at the recipient top (point T), TT [ºC] (*)	217	387	60 (@)	90 (@)

(#) Nearly forty trials were accomplished for gas temperature measurements at three points around the kettle
(*) At this point the thermocouple is reasonably shielded from the environment by the recipient bottom and the stove table
(@) At this point the thermocouple shielding is very pour (it sees the environment), so the values indicated are less representative of the real ones. Another possible cause for these low values is the air entrainment at the jet bend, where it passes from a radial jet to a vertical one, not taken into account in the mathematical model.

5. CONCLUSIONS

The use of shields jointly with treatments leading to high emissivity surfaces resulted considerable improvement into the efficiency of heat transfer from the flame to the recipients. This would imply significant reduction in the natural gas consumption for food cooking in industrial stoves.

The improvement in the efficiency for the same type of shield and the same surface treatment is higher for kettles due to their large ratio (lateral surface area to total external surface area) that is 0,794 against 0,646 for sauce pans. This can be verified comparing the results for configuration 9 (kettle) and 11 (sauce pan) which correspond to the same kind of shield and surface treatment.

The improvement in surfaces emissivity used in the experimental work consisted in the deposition of a soot layer by the impingement of a reducing acetylene-oxygen flame, resulting very high emissivities (around 0,95). Obviously this is not feasible for kitchen ware in which case the most common solution is to anodize the surfaces using coating thickness around 10 microns which allows emissivity values around 0,8, according to G.E. (1978) and EOI (2000).

6. REFERENCES

Page, R.H., Ostowari, C., Hadden, L.L. “A theory for radial jet reattachment flow”. AIAA – 1988 – 3589-CP. In: ASME, SIAM and APS, National Fluid Dynamics Congress, 1st, Cincinnati, OH, July 25-28, 1988, Technical Papers. Part 2 (A88 -48776 20-34). Washington, DC, American Institute of Aeronautics and Astronautics, 1988, p.925—931.

Ostowari, C., Page, R.H., Paikert, B. “Heat transfer measurements of radial jet reattachment of a flat plate”. AIAA – 1988 – 3772. In: ASME, SIAM and APS, National Fluid Dynamics Congress, 1st, Cincinnati, OH, July 25-28, 1988, Technical Papers. Part 3 (A88 -48776 20-34). Washington, DC, American Institute of Aeronautics and Astronautics, 1988, p.1901—1907.

Abramovich, G.N. “The Theory of Turbulent Jets”, The Massachussets Institute of Technology, 1963.

Sawyer, R.A. “Two-dimensional reattaching jet flows including the effects of curvature on entrainment”. Journal of Fluid Mechanics, 17, 1963, pp. 481-498.

Hottel, H.C. and Sarofim, A.F. “Radiative Transfer”, McGraw-Hill, 1967.

Howell, J.R., site at internet with diagrams and grafics for radiation exchange factors: http://www.me.utexas.edu/~howell/tablecon.html

EN 203-1:2005, “Gas heated catering equipment”

EN 203-2-1:2006 “Gas heated catering equipment - Part 2-1: Specific requirements – open burners and wok burners”

NBR 13.723:1996 “Aparelho doméstico de cocção a gás – Parte 1:desempenho e segurança”

NBR 13.723-2 “Aparelho doméstico de cocção a gás – Parte 2: Uso Racional de Energia”

EOI – Electro Optical (2000) – internet site:http://www.electro-optical.com/bb_rad/emissivity/matlemisivty.htm

General Electric Co, Corporate Research and Development, “Heat Transfer and Fluid Flow Data Books” (1978)

Sousa, F.D.A. and Hua, Ding, “Uso eficiente de gás natural em fogões”, Relatório Técnico IPT Nº 108804-205, março/2009.